INTERNATIONAL JOURNAL FOR NUMERICAL METHODS IN FLUIDS
Int. J. Numer. Meth. Fluids 2008; **58**:879–896
Published online 17 March 2008 in Wiley InterScience (www.interscience.wiley.com). DOI: 10.1002/fld.1773

A further work on multi-phase two-fluid approach for compressible multi-phase flows

Yang-Yao Niu[1,*,†,‡], Yu-Chin Lin[1] and Chih-Hao Chang[2]

[1]*Institute of Mechanical and Aerospace Engineering, Chung-Hua University, Hsin- Chu, Taiwan, Republic of China*
[2]*Center for Risk Studies and Safety, University of California, Santa Barbara, Santa Barbara, CA, U.S.A.*

SUMMARY

This paper is to continue our previous work Niu (*Int. J. Numer. Meth. Fluids* 2001; **36**:351–371) on solving a two-fluid model for compressible liquid–gas flows using the AUSMDV scheme. We first propose a pressure–velocity-based diffusion term originally derived from AUSMDV scheme Wada and Liou (*SIAM J. Sci. Comput.* 1997; **18**(3):633—657) to enhance its robustness. The scheme can be applied to gas and liquid fluids universally. We then employ the stratified flow model Chang and Liou (*J. Comput. Physics* 2007; **225**:240–873) for spatial discretization. By defining the fluids in different regions and introducing inter-phasic force on cell boundary, the stratified flow model allows the conservation laws to be applied on each phase, and therefore, it is able to capture fluid discontinuities, such as the fluid interfaces and shock waves, accurately. Several benchmark tests are studied, including the Ransom's Faucet problem, 1D air–water shock tube problems, 2D shock-water column and 2D shock-bubble interaction problems. The results indicate that the incorporation of the new dissipation into AUSM$^+$-up scheme and the stratified flow model is simple, accurate and robust enough for the compressible multi-phase flows. Copyright © 2008 John Wiley & Sons, Ltd.

Received 5 March 2007; Revised 10 December 2007; Accepted 1 January 2008

KEY WORDS: AUSMDV; two-fluid model; multi-phase flow; pressure–velocity coupling; shock waves; material interfaces

INTRODUCTION

In many industrial mechanisms, fluids usually appear in states of multiple phases or components. One could classify them according to the states of different phases or components such as the so-called gas–solid, liquid–solid, gas–particle or bubbly flows, and so on. These multi-phase flows

*Correspondence to: Yang-Yao Niu, Institute of Mechanical and Aerospace Engineering, Chung-Hua University, Hsin- Chu, Taiwan, Republic of China.
†E-mail: yniu@chu.edu.tw
‡Professor.

are widely seen in engineering applications such as the power cooling system, fuel transport system, underwater cavitation problems and droplet erosion problems. For example, as we know, in the cooling system within the convectional nuclear reactor, the high-pressure water is transported through pipes and pumps. Once a break occurs in the pipe, there will be a sudden depressurization and the water will begin to evaporate, hence presenting a very high risk to damage the systems. Clearly, the capability to predict the flow behavior of these processes is a very important subject in modern industry.

One widely accepted approach to fluids containing individual particles, droplets or bubbles is through the so-called two-fluid model, in which the time or space ensemble average process is applied to both continuous and disperse phases [1, 2]. Two sets of Navier–Stokes equations are used to describe both phases of fluids with additional inter-phasic terms for the exchange of momentum and energy between phases. Since each phase has its own velocity and temperature, the two-fluid model allows both mechanical and thermal non-equilibriums to be taken into account, and in that respect, it represents a more general model for two-phase flows.

However, the two-fluid model also brings difficulties for numerical simulation. One of the issues is its non-hyperbolicity, making the system an ill-posed problem, which can be presented as numerical instability. Additional terms or assumptions, such as the interfacial pressure force [3], virtual mass force [4] and the two-pressure model [5], have to be used to render the system of equations hyperbolic. Even though the system is hyperbolic, it is difficult to derive the analytical form of its eigensystem. Hence, this disadvantage prevents it from being solved by some modern upwind schemes.

Another concern is the appearance of the fluid interface that always considers the large disparity in materials' properties (about almost 5 times difference in sound speed and 1000 times difference in density between water and air), it demonstrates considerable difficulty in numerical simulation. Different from other interface tracking methods, such as the level set method [6] and volume of fluid method [7, 8], which use auxiliary transport function to track the fluid interface, however, the two-fluid model [5, 9, 10] treats the interface as a weak solution in the fluid. The interface is captured by ensuring the conservation law. The problem is that the two-fluid model is not in conservative form. The presence of non-conservative terms in momentum equations can cause the solution to oscillate in the vicinity of interface. It requires some non-standard discretization methods to ensure the exact capturing of the interface.

In this paper, we will continue our studies in using the AUSM-family scheme to solve the multi-phase flows. The AUSM$^+$ scheme proposed by Liou [11] is well known to be as accurate as Roe's or Osher's approximate Riemann solvers without the cost of field-by-field wave decompositions, which makes it amenable to the two-fluid model since its eigensystem is difficult to be expressed in analytical form. Of particular importance is the capability of the scheme to capture contact discontinuities exactly, thereby making the scheme very attractive for resolutions of fluid interfaces.

Edwards *et al*. [12] first extended the AUSM$^+$ scheme to solve multi-phase flow based on a homogeneous mixture model, which assumes that all phases are in kinematics and thermodynamic equilibrium and use one set of Navier–Stokes equations. The extension utilizes additional dissipation terms obtained from the early AUSMDV scheme by Wada and Liou [13] to enhance its stability in low Mach number flow. The scheme is classified as AUSM$^+$-up scheme for the extra velocity and pressure dissipation terms. Niu [8, 9] later implemented the AUSMDV scheme to solve a seven-equation two-fluid model involving two sets of Navier–Stokes equations and one non-conservative transport equation for volume fraction. It is found that the non-conservative transport equation can easily cause unwanted numerical instability and errors. Based on that, the

DOI: 10.1002/fld

efforts embarked on the modification of the AUSM-type scheme to solve the two-fluid model are still continued. The first successful work was performed by Paillère *et al.* [14] on the six-equation two-fluid model using modified AUSM$^+$ scheme. Subsequently, Chang and Liou [10, 15] proposed the AUSM$^+$-up scheme incorporating with the stratified flow model to discretize the system equations. The stratified flow model was suggested by Stewart and Wendroff [16]. It was noted that the governing equations for the stratified flows are equivalent to those of the two-fluid model under certain conditions. By considering fluids as immiscible and being separated from each other, it makes the stratified flow model more preferable for the finite volume method, since we can apply conservative law to each fluid simultaneously. Their approach demonstrates robustness and high-order accuracy in their benchmark cases. However, they used the exact Riemann solver to calculate the numerical fluxes between different fluids. Since the exact Riemann solver requires extensive iterations, it is much more CPU time consuming than other methods, especially when stiff EOS of fluid (such as the stiffened gas model for water) is used.

Besides, in our previous study on the mixture model [8, 9], it is found that we can enhance the resolution of the fluid interface and pressure waves within liquid phase by adding some extra pressure–density ratio terms [13] to the original AUSM$^+$-up scheme. In this study, we would like to replace the exact Riemann solver by the new AUSM$^+$-up scheme. We expect that the new scheme can effectively improve the efficiency and still be as robust and accurate as using the exact Riemann solver. Several benchmark test problems, including the Ransom's faucet problem [17], 1D air–water shock tube problems and a 2D gaseous shock-water column interaction problem, will be chosen for validation.

NUMERICAL MODELS

In this section, the system equations of the two-fluid model are described. The related spatial and time discretization of the model equations solved by the new AUSM$^+$-up scheme is also introduced. A detailed discussion on the stratified flow method can be found in Chang and Liou [10].

Governing equations

Here, the single pressure six-equation models expressed in the hyperbolic form [14, 15] is

$$\frac{\partial U}{\partial t}+\frac{\partial E}{\partial x}=S \tag{1}$$

with

$$U=\begin{bmatrix}\alpha_g\rho_g\\ \alpha_l\rho_l\\ \alpha_g\rho_g u_g\\ \alpha_l\rho_l u_l\\ \alpha_g\rho_g E_g\\ \alpha_l\rho_l E_l\end{bmatrix},\quad E=\begin{bmatrix}\alpha_g\rho_g u_g\\ \alpha_l\rho_l u_l\\ \alpha_g\rho_g u_g^2+\alpha_g p\\ \alpha_l\rho_l u_l^2+\alpha_l p\\ \alpha_g\rho_g u_g H_g\\ \alpha_l\rho_l u_l H_l\end{bmatrix},\quad S=\begin{bmatrix}0\\ 0\\ g_x\cdot\alpha_g\cdot\rho_g+F_g^{\mathrm{d}}+p_{int}\cdot\nabla\alpha_g\\ g_x\cdot\alpha_l\cdot\rho_l+F_l^{\mathrm{d}}+p_{int}\cdot\nabla\alpha_l\\ -p\dfrac{\partial\alpha_g}{\partial t}+g_x\cdot\alpha_g\cdot\rho_g\cdot u_g\\ -p\dfrac{\partial\alpha_l}{\partial t}+g_x\cdot\alpha_l\cdot\rho_l\cdot u_l\end{bmatrix} \tag{2}$$

DOI: 10.1002/fld

where U is the vector of conserved variables, E is the corresponding convective flux vector and S is the vector of the interfacial source terms including the interface pressure correction terms, gravity and the interfacial drag term F_k^{d} with $k=g,l$. The subscripts g and l represent the gas and liquid phases, respectively. Also, the interfacial drag term considers the drag caused by the momentum exchange between two phases. α stands for the phase volume fraction, and ρ, u and E are density, velocity and total energy for each phase, respectively. The total energy $E_k=e_k+\frac{1}{2}u_k$, where e is denoted by the internal energy. The enthalpy $H=E+p/\rho$. Here, we neglect viscous terms, also assuming that no phase change occurs between the air and the liquid phases. The interfacial pressure p^{int} was originally used to resemble the averaged pressure over the particle surface in dispersed flows (particulate or bubbly flows). It can be expressed in a general form as in [14] like:

$$p_{\mathrm{int}}=p-\sigma\frac{\alpha_g\rho_g\alpha_l\rho_l}{\alpha_g\rho_l+\alpha_l\rho_g}(u_g-u_l)^2 \tag{3}$$

where it is designed to make the system equations to be hyperbolic and well posed when the constant $\sigma\geqslant 1$ as suggested by Stuhmiller [3] for low-speed flows. Recently, the work of Chang *et al*. [18] pointed out the necessary conditions for hyperbolic system for high-speed flow. In their paper, it is noted that $\sigma=2$ is adequate for most of test cases. Also, the interface drag terms are chosen as

$$F_g^{\mathrm{d}}=C_f\alpha_g(\alpha_g-1)\rho_g(u_g-u_l) \quad \text{and} \quad F_l^{\mathrm{d}}=-F_g^{\mathrm{d}}$$

with a positive constant C_f (1/s). Here, we used C_f as 10^{-6} to weaken the numerical instability which may be produced from the drag force.

In this work, the system equations are closed by equations of states, and the gas and liquid fluids are governed by the perfect gas and stiffened gas models, respectively.

Equation of state

For the gas phase,

$$P_g=\rho_g R_g T_g, \quad e_g=\frac{R_g}{\gamma_g-1}T_g \tag{4}$$

Here, the parameters used for specifying the thermodynamic properties of vapor are

$$\rho_g=1\,\mathrm{kg/m^3}, \quad \gamma_g=1.4, \quad R_g=288.2\,\mathrm{kg/K}$$

and the speed of sound is

$$a_g=\left(\frac{\gamma_g P}{\rho_g}\right)^{1/2} \tag{5}$$

For the water, the stiffened gas model proposed by Harlow and Amsden [19] is adopted as

$$p_l=\frac{\gamma_l-1}{\gamma_l}\rho_l C_{pl}T_l-p_\infty, \quad e_l=\frac{C_{pl}}{\gamma_l}T_l+\frac{p_\infty}{\rho_l} \tag{6}$$

and the speed of sound is

$$a_l=\left(\frac{\gamma_l(p_l+p_\infty)}{\rho_l}\right)^{1/2} \tag{7}$$

DOI: 10.1002/fld

Here, the parameters used for specifying the thermodynamic properties of water are determined to meet the following criteria. When $T_l = 293.15\,\mathrm{K}$ and $P = 1.0132 \times 10^5\,\mathrm{Pa}$, we set the following properties based on the data:

$$\gamma_l = 1.932, \quad C_{pl} = 8095.08\,\mathrm{J/kg\,K}, \quad P_\infty = 1.1645 \times 10^9\,\mathrm{Pa}$$

Note that the existence of the huge constant p_∞ represents a very weak link between pressure and density function. The density will remain almost unchanged even when a very big pressure is applied. Therefore, how to enhance the coupling between pressure and density field is a key point to achieve accurate modeling of low-speed compressible liquid flow.

Before performing numerical flux calculations, we need to know the primitive variable as

$$V = \begin{bmatrix} \alpha_g \\ u_g \\ u_l \\ p \\ T_g \\ T_l \end{bmatrix} \tag{8}$$

The transformation matrix between the vectors of the primitive and conservative variables can be expressed as $V = \phi(U)$ based on

$$U = \begin{bmatrix} \alpha_g \rho_g \\ \alpha_l \rho_l \\ \alpha_g \rho_g u_g \\ \alpha_l \rho_l u_l \\ \alpha_g \rho_g E_g \\ \alpha_l \rho_l E_l \end{bmatrix} \tag{9}$$

After solving the non-linear system equation $\phi(U) = 0$, we can have

$$u_g = \frac{U_3}{U_1}, \quad u_l = \frac{U_4}{U_2}, \quad e_g = \frac{U_5}{U_1} - \frac{1}{2}\left(\frac{U_3}{U_1}\right)^2 \quad \text{and} \quad e_l = \frac{U_6}{U_2} - \frac{1}{2}\left(\frac{U_4}{U_1}\right)^2 \tag{10}$$

with

$$U_1 = \alpha_g \rho_g(p, T) \tag{11}$$

and

$$U_2 = (1 - \alpha_g)\rho_l(p, T) \tag{12}$$

To achieve the common pressure between different phases, we can substitute (11) into (12) to eliminate α_g; also substituting into Equations (4) and (6), a non-linear equation $F(p) = 0$ is achieved as

$$p^2 + [\gamma_l p_\infty - U_1(\gamma_g - 1)e_g - U_2 p(\gamma_l - 1)e_l]p - U_1(\gamma_g - 1)e_g \gamma_l p_\infty = 0 \tag{13}$$

DOI: 10.1002/fld

The pressure can be easily obtained by solving Equation (13) based on the Newton–Raphson iteration method. Then the volume fractions of both phases can be achieved after the pressure is known as

$$\alpha_g = \frac{U_1(r_g - 1)e_g}{p} \tag{14}$$

and

$$\alpha_l = 1 - \alpha_g \tag{15}$$

Also, the density of each phase can be achieved differently as

$$\rho_g = \frac{U_1}{\alpha_g} \tag{16}$$

and

$$\rho_l = \frac{U_2}{\alpha_l} \tag{17}$$

Finally, the temperature of each phase can be computed as follows:

$$T_g = \frac{r_g - 1}{R_g} e_g \tag{18}$$

and

$$T_l = \frac{r_l e_l (p + p_\infty)}{C_p (p + r_l p_\infty)} \tag{19}$$

Spatial and time discretization

For spatial discretization, the primitive variables on the cell interface are determined through the MUSCL-type approach with TVD minmod limiter, which can provide second- or third-order spatial accuracy [8]. In this paper, we found that there was no notable difference between solutions obtained from second- or third-order scheme. Only the interpolation results with the third-order spatial accuracy are presented. Once the primitive variables on the left and right of the cell interface are determined, we use the new AUSM$^+$-up scheme to calculate the numerical fluxes across the interface. The details of the new AUSM$^+$-up scheme are described in the following section.

Next, the TVD-type Rung–Kutta time marching method [20] is chosen to perform the time integration. Referring to the governing equations, it can be proceeded as

$$\begin{aligned} Q_k^{(1)} &= Q_k^n - \Delta t L(Q^n) \\ Q_k^{(2)} &= \tfrac{3}{4} Q_k^n - \tfrac{1}{4}[Q_k^{(1)} - \Delta t L(Q_k^{(1)})] \\ Q_k^{n+1} &= \tfrac{1}{3} Q_k^n + \tfrac{2}{3}[Q_k^{(2)} - \Delta t L(Q_k^{(2)})] \end{aligned} \tag{20}$$

DOI: 10.1002/fld

where

$$Q_k = \begin{pmatrix} \alpha_k \rho_k \\ \alpha_k \rho_k u_k \\ \alpha_k \rho_k E_k + p_{\text{int}}^{\text{s}} \alpha_k \end{pmatrix} \tag{21}$$

and

$$L(Q_k) = ((E_{i+1/2}^n(Q_{i+1/2}^L, Q_{i+1/2}^R) - E_{i-1/2}^n(Q_{i-1/2}^L, Q_{i-1/2}^R)) - S(Q_i^n)) \tag{22}$$

where $k = g, l$ and the superscript 's' in $p_{\text{int}}^{\text{s}}$ indicates the sub-step in the Runge–Kutta method. It should be cautioned to use the same $p_{\text{int}}^{\text{s}}$ everywhere within each sub-step to hold the conservation law. Otherwise, auxiliary oscillation in pressure field will be generated.

AUSM$^+$-up scheme

The basic ideal for the AUSM$^+$ scheme is to split the numerical flux into convection and pressure fluxes. Then a flux difference scheme is used to calculate the convection flux, and a flux splitting scheme is used for the pressure flux. We can express the numerical fluxes as

$$\begin{aligned} \mathbf{F} &= \mathbf{f}^{cv} + \mathbf{f}^{p} \\ &= a_{1/2} m_{1/2} \rho_{\text{L/R}} \boldsymbol{\psi}_{\text{L/R}} + \begin{pmatrix} 0 \\ p_{1/2} \\ 0 \end{pmatrix} \end{aligned} \tag{23}$$

and

$$\boldsymbol{\psi} = (1, u, uH)^{\text{T}} \tag{24}$$

The subscript 'L/R' means the variables are chosen in an upwind manner. For example, if $m_{1/2} \geqslant 0$, then $\rho_{\text{L/R}} = \rho_{\text{L}}$; otherwise $\rho_{\text{L/R}} = \rho_{\text{R}}$. The $a_{1/2}$ is the mean speed of sound. Here we simply use simple average:

$$a_{1/2} = \tfrac{1}{2}(a_{\text{R}} + a_{\text{L}}) \tag{25}$$

Then we can define the Mach number for left and right states:

$$M_{\text{L}} = \frac{u_{\text{L}}}{a_{1/2}} \quad \text{and} \quad M_{\text{R}} = \frac{u_{\text{R}}}{a_{1/2}} \tag{26}$$

The splitting functions $m_{1/2}$ and $p_{1/2}$ are defined as

$$m_{1/2} = \mathsf{M}_{(4)}^{+}(M_{\text{L}}) + \mathsf{M}_{(4)}^{-}(M_{\text{R}}) \tag{27}$$

$$p_{1/2} = P_{(5)}^{+}(M_{\text{L}}) + \mathsf{P}_{(5)}^{-}(M_{\text{R}}) \tag{28}$$

DOI: 10.1002/fld

with

$$\mathsf{M}^{\pm}_{(4)}(M)=\begin{cases}\pm(M\pm1)^2\pm(M^2-1)^2, & |M|<1\\ \mathsf{M}^{\pm}_{(1)}(M) & \text{otherwise}\end{cases} \tag{29}$$

$$\mathsf{P}^{\pm}_{(5)}(M)=\begin{cases}\frac{1}{4}(M\pm1)^2(2\mp M)\pm\frac{3}{16}M(M^2-1)^2, & |M|<1\\ (1/M)\mathsf{M}^{\pm}_{(1)}(M) & \text{otherwise}\end{cases} \tag{30}$$

and

$$\mathsf{M}^{\pm}_{(1)}(M)=\tfrac{1}{2}(M\pm|M|) \tag{31}$$

where the subscripts '(1)', '(4)' and '(5)' mean the orders of the polynomial of the splitting functions.

The AUSM$^+$ scheme has been proven to be very robust and accurate for compressible gas flows. However, in order to remove the odd–even decoupling errors at low-speed flows simulation, the AUSM$^+$ scheme was modified by adding two pressure–velocity-based dissipation terms to enhance the coupling between pressure and density field [12]. The same idea was later applied to solve compressible liquid flows [15]. The AUSMDV can be expressed in the AUSM$^+$-up scheme ('-up' indicates the pressure- and velocity-based dissipation terms) as

$$\mathbf{F}=(a_{1/2}m_{1/2}\rho_{\mathrm{L/R}}+D_p)\boldsymbol{\psi}_{\mathrm{L/R}}+\begin{pmatrix}0\\ p_{1/2}+D_u\\ 0\end{pmatrix} \tag{32}$$

with

$$D_p=\frac{\rho_{\mathrm{L}}\rho_{\mathrm{R}}}{p_{\mathrm{L}}\rho_{\mathrm{R}}+p_{\mathrm{R}}\rho_{\mathrm{L}}}\begin{bmatrix}(\delta\mathsf{M}^{+}(M_{\mathrm{L}})-\delta\mathsf{M}^{-}(M_{\mathrm{R}}))(p_{\mathrm{L}}-p_{\mathrm{R}})\\ +(\delta\mathsf{M}^{+}(M_{\mathrm{L}})+\delta\mathsf{M}^{-}(M_{\mathrm{R}}))(p_{\mathrm{L}}+p_{\mathrm{R}})\end{bmatrix} \tag{33}$$

$$D_u=\mathsf{P}^{+}_{(5)}(M_{\mathrm{L}})\mathsf{P}^{-}_{(5)}(M_{\mathrm{R}})\rho_{1/2}a_{1/2}(u_{\mathrm{L}}-u_{\mathrm{R}}) \tag{34}$$

and

$$\delta\mathsf{M}^{\pm}(M)=(\mathsf{M}^{\pm}_{(4)}(M)-\mathsf{M}^{\pm}_{(1)}(M)) \tag{35}$$

We should point out here that the dissipation terms D_p and D_u are designed to imitate the dissipation terms of the AUSMDV scheme proposed by Wada and Liou [13]. The above formulation (Equations (32)–(35)) had been implemented in [12]. Incorporating with time pre-conditioning method, the accuracy and robustness in solving all-speed gas flow problems are demonstrated. It is noted that the pre-conditioning technique is necessary to ease the stiffness of the eigensystem when Mach number approaches zero. Later Chang and Liou [15] proposed other forms of D_p and D_u which allow the scheme to work on very stiff system, such as water flows governed by stiffened gas model without using time preconditioning. They gave

$$D_p=\kappa_p\frac{\Delta\mathsf{M}\cdot\max(1-\overline{M}^2,0)\cdot(p_{\mathrm{L}}-p_{\mathrm{R}})}{a_{1/2}} \tag{36}$$

$$D_u=\kappa_u\mathsf{P}^{+}_{(5)}(\overline{M}_{\mathrm{L}})\mathsf{P}^{-}_{(5)}(\overline{M}_{\mathrm{R}})\rho_{1/2}a_{1/2}(u_{\mathrm{L}}-u_{\mathrm{R}}) \tag{37}$$

DOI: 10.1002/fld

with

$$\Delta \mathsf{M} = \mathsf{M}^{+}_{(4)}(M_{\mathrm{L}}) - \mathsf{M}^{+}_{(1)}(M_{\mathrm{L}}) - \mathsf{M}^{-}_{(4)}(M_{\mathrm{R}}) + \mathsf{M}^{-}_{(1)}(M_{\mathrm{R}})$$
$$= \delta \mathsf{M}^{+}(M_{\mathrm{L}}) - \delta \mathsf{M}^{-}(M_{\mathrm{R}}) \tag{38}$$

and

$$\overline{M} = \tfrac{1}{2}(M_{\mathrm{L}} + M_{\mathrm{R}}) \tag{39}$$

Usually the coefficients $\kappa_p = \kappa_u = 1$ are chosen for most of the cases. The above scheme (Equation (32), (36) and (37)) shows very good capability to capture pressure wave in either gas or liquid flows. However, it gives auxiliary oscillation when large disparity of material properties is present between both sides of the interface [15], such as the resolution of the gas–liquid interface. Therefore, Chang and Liou [10] suggested using the exact Riemann solver to calculate the numerical fluxes across the gas–liquid interface and it showed very good results in simulating flows with complex shock-interface interactions. The only problem is that the exact Riemann solver needs extensive iterations, hence making it very time consuming.

In order to avoid using the exact Riemann solver, we keep trying to enhance the stability of AUSM^{+}-up scheme and wish the same scheme can be applied to all the gas–gas, liquid–liquid and gas–liquid interfaces consistently. First, we find if we replace the Mach splitting function $m_{1/2}$ defined in Equation (27) by

$$m_{1/2} = \mathsf{M}^{+}_{(1)}(M_{\mathrm{L}}) + \mathsf{M}^{-}_{(1)}(M_{\mathrm{R}}) \tag{40}$$

we can enhance the dissipation when M approaches zero.[§] Next we take part of the pressure dissipation D_p of Equation (32) and rewrite it as

$$D_p = \frac{\rho_{\mathrm{L}}\rho_{\mathrm{R}}}{p_{\mathrm{L}}\rho_{\mathrm{R}} + p_{\mathrm{R}}\rho_{\mathrm{L}}} \Delta \mathsf{M} \cdot \max(1 - \mathrm{int}(\overline{M}^2), 0) \cdot (p_{\mathrm{L}} - p_{\mathrm{R}}) \tag{41}$$

where the function int$(\cdot)$ is the so-called integer truncated function that transforms the real number into a biggest integer number smaller than it. This slight modification on mass flux can work very well on either pure gas, pure liquid or gas–liquid flows at every transient states [21].

NUMERICAL APPLICATIONS

Ransom's faucet problem

We consider a simplified faucet flow problem proposed by Ransom [17]. As shown in Figure 1, the water 'faucet' problem consists of a liquid stream with a fixed inflow rate of water at a velocity of 10.0 (m/s), temperature of 300 K and a liquid volume fraction of 0.8 entering a vertical tube 12.0 m in length and 1.0 m in diameter from the top. Owing to the action of gravity, the water falls to form a stream of uniformly decreasing cross-section. The bottom of the tube is opened to the ambient pressure. Also simple extrapolations of inflow and outflow boundary conditions are applied. Wall fraction and inter-phasic friction are not considered in this case.

[§] It can be shown that the numerical dissipation of the convection flux in Equation (23) changes from $O(M^2)$ to $O(M)$ when using the splitting function of Equation (40) instead of Equation (27).

DOI: 10.1002/fld

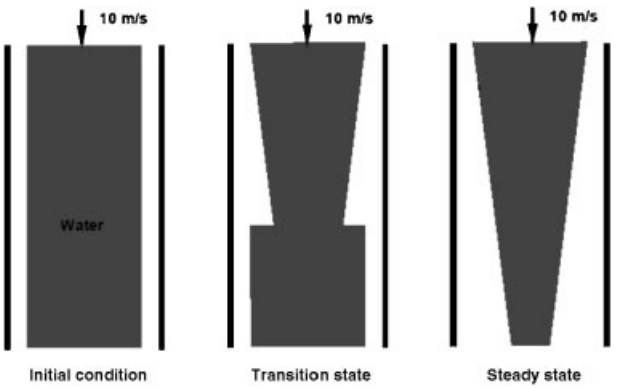

Figure 1. Illustration of Ransom's water faucet problem.

As we know, Ransom's problem is a widely used benchmark test to verify the accuracy of the two-fluid models and schemes. The previous works [9, 12, 14, 22] on the computations of this problem always generated smeared or oscillatory wavefront of void fraction. Chang and Liou [10] pointed out that one reason for such an oscillation is due to the discretization of the space differential terms, especially the inter-phasic term $p_{\text{int}}\nabla\alpha$ (the last term in Equation (2)). If we consider a contact discontinuity moving with constant velocity and constant pressure, one necessary condition to capture the discontinuity exactly is to discretize the inter-phasic term in a way that all pressure forces can be canceled, or the so-called non-disturbing pressure condition. By doing so, the equations can be reduced to a simple convection equation. Otherwise, the residues generated by the pressure terms will interfere with the flows and cause oscillation when the void fraction varies.

For Ransom's problem, the flow driven by gravity and pressure is almost unchanged over the domain. By satisfying the pressure non-disturbing condition, the stratified flow model we used for discretization is shown to minimize the disturbance caused by pressure terms. However, we still need additional mechanisms to regularize the flows, such as the interfacial pressure correction term presented in Equation (2) as noted by Stuhmiller [3].

Figure 2 demonstrates how σ takes effect in the simulation. Void function profiles calculated by different σ's are applied. According to Givler [23], '*the interfacial pressure is diffusive*..., *it leads to a homogenizing of the particle concentration field*; *local increases in particle concentration produces a momentum flux which opposes the concentration gradient*'. When $\sigma = 0$, the two-fluid model is ill-posed mathematically. Although the wavefront is sharply captured, the oscillation is still shown in the profile. By increasing σ, we find the void fraction profile is smeared, indicating that diffusive mechanism is able to control the oscillation and regularize the flow effectively. In Figure 3, the grid independence study is performed. It is shown that the computed results on the mesh cells of 500 and 1000 are identical. Therefore, we used the 500 grid points for this case. In addition, the comparison of computed results by the old version as Equations (27), (32) and (36) and new version as Equations (32) and (40), (41) is demonstrated in Figure 4. It can be found that the unwanted oscillation around the void fraction wavefront is really reduced by the new version. In Figure 5, we show the computed time evolution of the void fraction propagation. The result compares very well with the analytical solution at different times.

DOI: 10.1002/fld

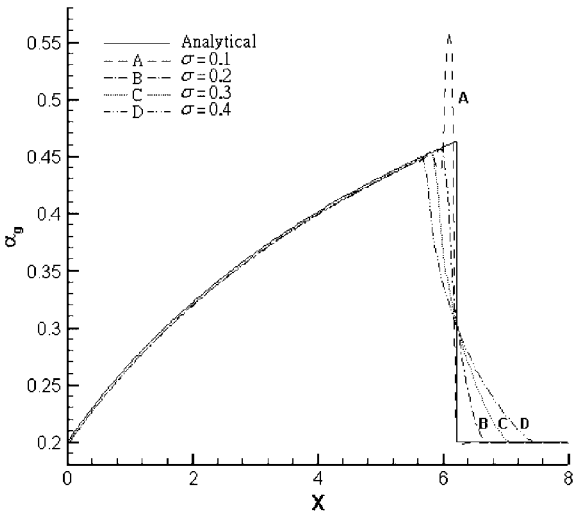

Figure 2. The void fraction profiles based on different σ's in the water faucet problem.

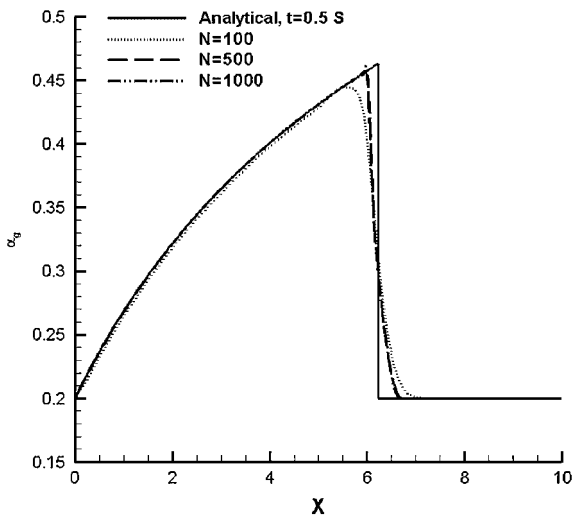

Figure 3. Several different grids are used in the water faucet problem.

1D air–water shock tube problem

Subsequently, we consider the test case described in the papers of Toumi and Kumbaro [22]. The fluid states in each side of the diaphragm are defined as

$$(p, \alpha_g, u_i, T_i)_{\mathrm{L}} = (2.0 \times 10^7\,\mathrm{Pa}, 0.25, 0\,\mathrm{m/s}, 308.15\,\mathrm{K})$$

$$(p, \alpha_g, u_i, T_i)_{\mathrm{R}} = (1.0 \times 10^7\,\mathrm{Pa}, 0.10, 0\,\mathrm{m/s}, 308.15\,\mathrm{K})$$

DOI: 10.1002/fld

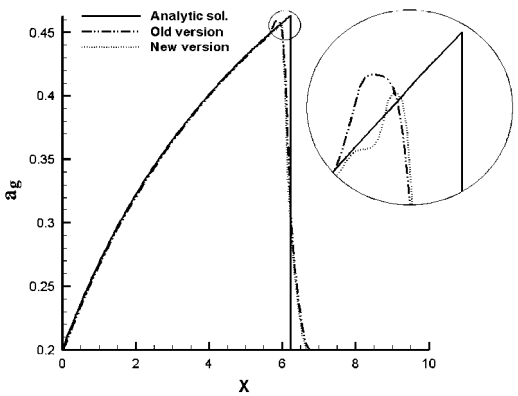

Figure 4. Calculations of the water faucet problem using different versions of AUSM$^+$-up.

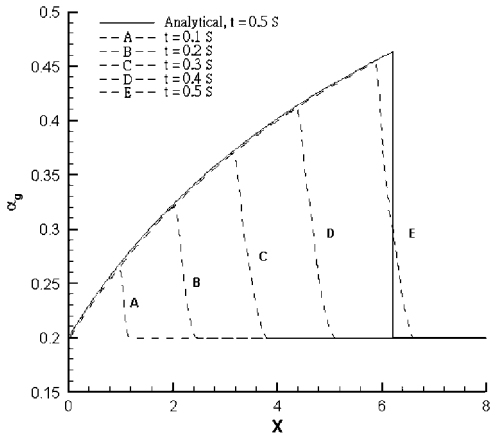

Figure 5. Time evolution of the void fraction profile in the water faucet problem.

The simulated results are shown in Figure 6(a) with $\sigma = 2.0$ and Courant–Friedrichs–Lewy (CFL) $= 0.5$. Several different grids of 100, 500, 1000, 2000 and 4000 cells are used for the computation. Only the computed results by the new AUSM$^+$-up are demonstrated. We observe no oscillatory behavior around the results. However, a slight difference between the interfaces in the resolution of void fraction wave is visible. Also, significant overshoots can be found in the transition region. Based on the analysis of Toumi, the eigenvalues include two expansion waves, two contact discontinuity and two shock waves. However, we capture only five distinct regions in Figure 6(a). However, this is consistent with the numerical results by Chang and Liou [10, 15]. Therefore, all of the shock waves, rarefaction waves and the fluid interfaces are sharply captured. Only slight oscillation can be found after the shock wave. There is no oscillation in the vicinity of the fluid interface.

DOI: 10.1002/fld

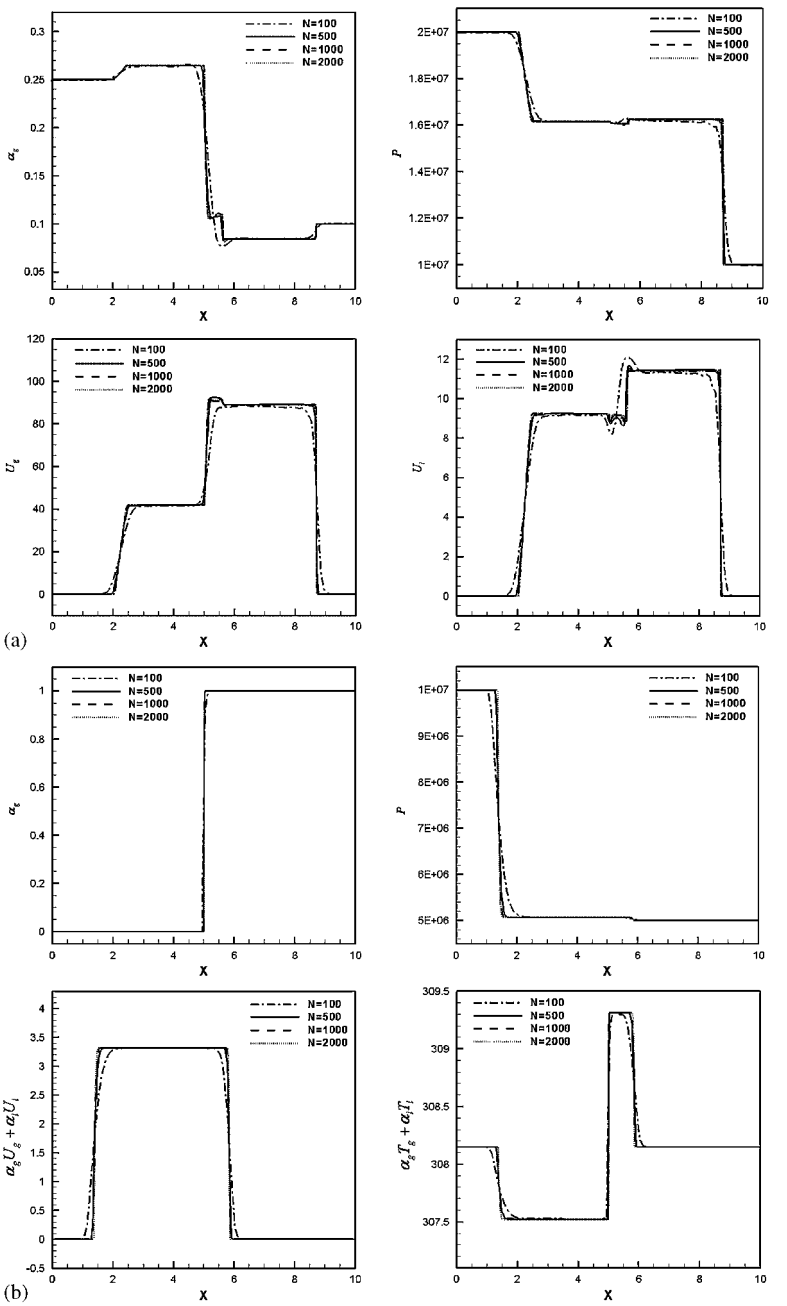

Figure 6. Profiles of the 1D air–water shock tube problem. The initial conditions are: (a) $(p, \alpha_g, u_i, T_i)_{\mathrm{L}} = (2.0 \times 10^7\,\mathrm{Pa},\ 0.25, 0\,\mathrm{m/s}, 308.15\,\mathrm{K})$ and $(p, \alpha_g, u_i, T_i)_{\mathrm{R}} = (1.0 \times 10^7\,\mathrm{Pa},\ 0.10, 0\,\mathrm{m/s}, 308.15\,\mathrm{K})$ and (b) $(p, \alpha_g, u_i, T_i)_{\mathrm{L}} = (1.0 \times 10^7\,\mathrm{Pa},\ \varepsilon, 0\,\mathrm{m/s}, 308.15\,\mathrm{K})$ and $(p, \alpha_g, u_i, T_i)_{\mathrm{R}} = (5.0 \times 10^6\,\mathrm{Pa}, 1-\varepsilon,\ 0\,\mathrm{m/s}, 308.15\,\mathrm{K})$.

DOI: 10.1002/fld

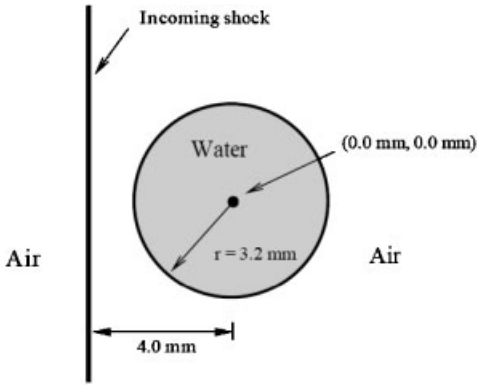

Figure 7. Illustration of the shock-water column interaction problem.

Next, we change the initial condition so that the shock wave propagates from the water side to the air. We have

$$(p, \alpha_g, u_i, T_i)_{\mathrm{L}} = (1.0 \times 10^7\,\mathrm{Pa}, \varepsilon, 0\,\mathrm{m/s}, 308.15\,\mathrm{K})$$

$$(p, \alpha_g, u_i, T_i)_{\mathrm{R}} = (5.0 \times 010^6\,\mathrm{Pa}, 1-\varepsilon, 0\,\mathrm{m/s}, 308.15\,\mathrm{K})$$

The results are shown in Figure 6(b) with $\varepsilon = 10^{-6}$. It is seen that the shock wave transmits from air into water due to compressibility. However, the shock wave is very difficult to travel from water into air. Only a small fraction of the shock wave is transmitted into air, and a very strong rarefaction is generated from the fluid interface and traveling back into the water. It is shown that the shock wave in the air is smeared, and there is one undershoot in the pressure near the expansion wave. One possible reason is that the stiffened gas equation of state may not correctly reflect the water liquid physics. In the real situation, the liquid undergoing a strong expansion wave will be vaporized into the gas phase if the pressure is dropped under the saturation pressure. However, a negative pressure is easily obtained while computing the stiffened gas equation of state with the large pressure-like constant P_∞ inside. A more sophisticated and reliable equation of state will be highly required to avoid numerical instability caused by the estimated negative pressure.

Generally, the new version of the AUSM$^+$-up is shown to capture shock and rarefaction wave in both air and water flows very well. Accurate and consistent results are presented based on grid independence study.

2D shock-water column interaction problem

Here, we study a problem of a planar shock wave interacting with one cylindrical water columns. The configuration is shown in Figure 7. First, we have a planar water column (diameter 6.4 mm) at the origin and the incoming air shock wave at the position $x = -4.0$ mm. The initial condition is presented as

$$p = 1.0 \times 10^5\,\mathrm{Pa}, \quad u_i = v_i = 0\,\mathrm{m/s}, \quad T_i = 346.98\,\mathrm{K}$$

DOI: 10.1002/fld

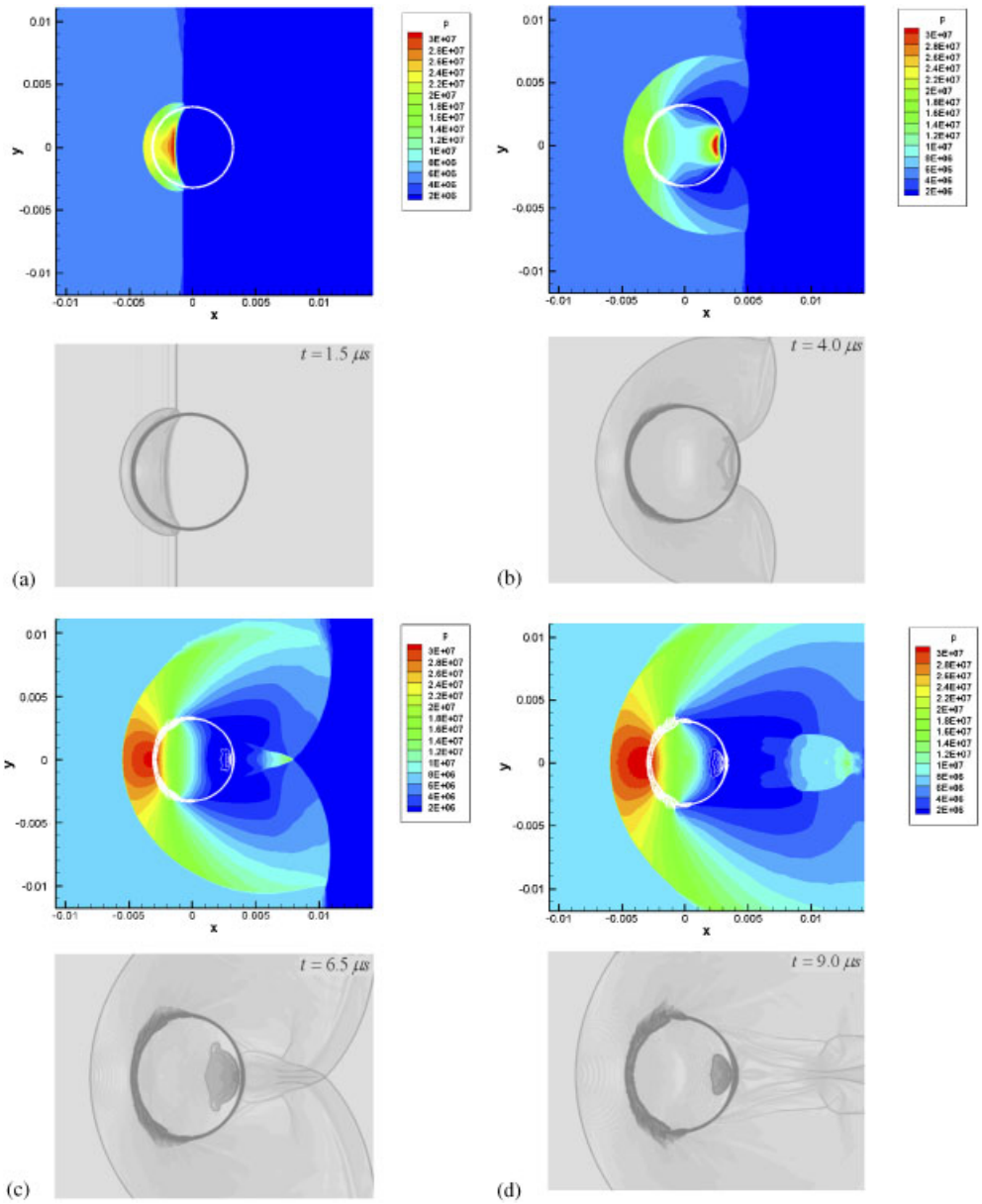

Figure 8. Time evolution of a shock-water column interaction problem (incoming shock speed is $M=6.0$). Contour of void fraction (white color) and pressure contours (other colors): (a) $t=1.5\,\mu s$; (b) $t=4.0\,\mu s$; (c) $t=6.5\,\mu s$; (d) $t=9.0\,\mu s$; (e) $t=11.5\,\mu s$; (f) $t=14.0\,\mu s$ (contours of function $\log(|\nabla\rho_{avg}|+1)$ (schlieren photo)).

DOI: 10.1002/fld

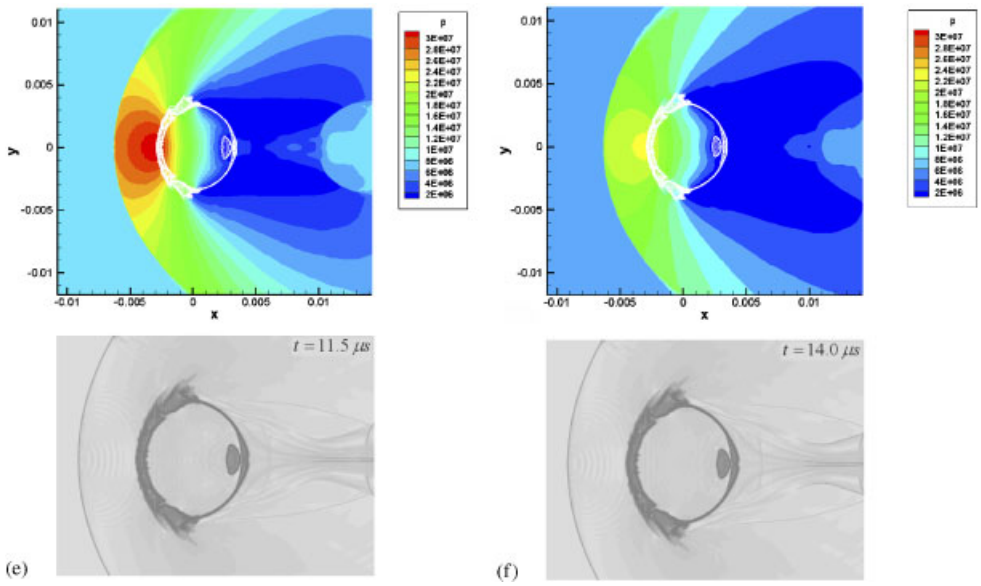

Figure 8. *Continued*.

and the states behind the shock are

$$p = 4.18375 \times 10^6\,\text{Pa}, \quad u_i = 1.818957 \times 10^3\,\text{m/s}, \quad v_i = 0\,\text{m/s}, \quad T_i = 2755.48\,\text{K}$$

The Mach number of the incident shock is 6.0, basically an incoming hypersonic shock wave. The Courant number CFL = 0.5 is chosen to maintain numerical stability. The computed results at transient states are presented in Figure 8. At $t = 1.5\,\mu\text{s}$, the shock speed of the air is found to be higher than the shock speed in the water column, despite that the sound speed of water is much higher than air as shown in Figure 8(a). The flow pattern of the reflected shock is similar to the shock reflected from a solid cylinder. In Figure 8(b), it is seen that the flow becomes unstable and the width of the fluid interface increases quickly as the incoming flow approaches the air–water interface at $t = 4.0\,\mu\text{s}$. It is observed that the shock within the water finally hits on the fluid interface in the rear side of the column and reflected as a rarefaction wave. The focused rarefaction waves create a very low pressure region. As the pressure approaches zero, the air begins to expand and creates a cavity-like structure in the rear of water column; even air takes only a very small fraction in our initial conditions (like assuming $\alpha_g = 10^{-6}$ within water). The cavity-like structure is shown inside the water column denoted by white color in pressure contours at $t = 6.5\,\mu\text{s}$ as shown in Figure 8(c). The area of the gas cavity becomes smaller and smaller as the flow evolves; the pressure in the cavity also drops dramatically at the same time. A complicated flow structure is developed in the interface when the air drags the water away from the interface as shown from Figure 8(c) to (f) (between $t = 6.5$ and $14.0\,\mu\text{s}$). It is shown that the developing interface interacting with the shock wave in front of the water column continuously creates a ripple-like flow pattern in the flow field.

DOI: 10.1002/fld

CONCLUSIONS AND SUGGESTIONS

In this work, the new version of AUSM$^+$-up is proposed to simulate multi-phase flows described by a six-equation two-fluid model with the stiffened gas model. The current scheme has been demonstrated accurate capturing the liquid pressure waves and the interfaces of the gas–liquid flows. However, a stiffened gas model is just a rough approximation to the liquid water. The pressure easily becomes negative when the liquid water flow undergoes a strong expansion wave and a vaporation. It indicates that a more precise equation of state is highly required for realistic applications.

ACKNOWLEDGEMENTS

The author also acknowledges fruitful discussions on the AUSM $^+$-up with Dr M. S. Liou from NASA John H. Glenn Research Center, U.S.A. The author wishes to acknowledge the computer facility support from the National Center for High-performance Computing, Taiwan.

REFERENCES

1. Buyevich YA. Statistical hydrodynamics for dispersed system, physical background and general equations. *Journal of Fluid Mechanics* 1971; **49**:489–507.
2. Ishii M. *Thermo-fluid Dynamic Theory of Two-phase Flow*. Eyrolles: Paris, 1975.
3. Stuhmiller JH. The influence of interfacial pressure forces on the character of two-phase flow model equations. *International Journal of Multiphase Flow* 1997; **3**:551–560.
4. Drew D, Cheng L, Lahey Jr RT. The analysis of virtual mass effects in two-phase flow. *International Journal of Multiphase Flow* 1979; **5**:233–242.
5. Saurel R, Abgrall R. A multiphase Godunov method for compressible multifluid and multiphase flows. *Journal of Computational Physics* 1999; **150**:425–467.
6. Sussman M, Smereka P, Osher S. A level set approach for computing solutions of incompressible two-phase flows. *Journal of Computational Physics* 1994; **114**:146–159.
7. Hirt W, Nichols BD. Volume of fluid method for the dynamics of free boundaries. *Journal of Computational Physics* 1981; **39**:201–225.
8. Niu Y-Y. Simple conservative flux splitting for multi-component flow calculations. *Numerical Heat Transfer, Part B* 2000; **38**:203–222.
9. Niu Y-Y. Numerical approximations of a compressible two fluid model by the advection upwind splitting method. *International Journal of Numerical Methods in Fluids* 2001; **36**:351–371.
10. Chang C-H, Liou M-S. A robust and accurate approach to computing compressible multiphase flow: stratified flow model and AUSM$^+$-up scheme. *Journal of Computational Physics* 2007; **225**:240–873.
11. Liou M-S. A sequel to AUSM: AUSM$^+$. *Journal of Computational Physics* 1996; **129**:364–382.
12. Edwards JR, Franklin RK, Liou M-S. Low-diffusion flux-splitting methods for real fluid flows with phase transitions. *AIAA Journal* 2000; **38**:1624–1633.
13. Wada Y, Liou M-S. An accurate and robust flux splitting scheme for shock and contact discontinuities. *SIAM Journal on Scientific Computing* 1997; **18**(3):633–657.
14. Paillère H, Corre C, García Cascales JR. On the extension of the AUSM$^+$ scheme to compressible two-fluid models. *Computers and Fluids* 2003; **32**:891–916.
15. Chang C-H, Liou M-S. A new approach to the simulation of compressible multifluid flows with AUSM$^+$ scheme. *AIAA Paper 2003–4107*, 2003.
16. Stewart HB, Wendroff B. Two-phase flow: models and methods. *Journal of Computational Physics* 1984; **56**:363–409.
17. Ransom VH. Numerical benchmark tests. In *Multiphase Science and Technology*, vol. 3, Hewitt GF, Delhaye JM, Zuber N (eds). Hemishpere Publishing Corporation: Berlin, 1987.
18. Chang C-H, Sushchikh S, Nguyen L, Liou M-S, Theofanous T. Hyperbolicity, discontinuities, numerics of two-fluid model. *Fifth Joint ASME/JSME Fluids Engineering Summer Conference*, San Diego, U.S.A., 30 July–2 August 2007.

DOI: 10.1002/fld

19. Harlow F, Amsden A. Fluid dynamics. *Technical Report LA-4700*, Las Alamos National Laboratory, 1971.
20. Su CW, Osher S. Efficient implementation of essentially non-oscillatory shock-capturing schemes. *Journal of Computational Physics* 1988; **77**:439–471.
21. Niu Y-Y, Lin Y-M, Lin Y-C. A simple and robust advection upwind flux splitting to simulate transient cavitated water-vapor flows. *Numerical Heat Transfer* 2007; **51**(7):679–696.
22. Toumi I, Kumbaro A. An approximate linearized Riemann solver for two-fluid model. *Journal of Computational Physics* 2006; **124**:286–300.
23. Givler RC. An interpretation for the solid-phase pressure in slow, fluid-particle flows. *International Journal of Multiphase Flows* 1987; **13**(5):717–722.

DOI: 10.1002/fld